Electrochemical noise measurements of steel corrosion in the molten NaCl-K2SO4 system

Cappeln, Frederik Vilhelm; Bjerrum, Niels; Petrushina, Irina

Published in:
Journal of The Electrochemical Society

Link to article, DOI:
10.1149/1.1928187

Publication date:
2005

Document Version
Publisher's PDF, also known as Version of record

Journal of The Electrochemical Society, **152** (7) B228-B235 (2005)
0013-4651/2005/152(7)/B228/8/$7.00 © The Electrochemical Society, Inc.

Electrochemical Noise Measurements of Steel Corrosion in the Molten NaCl-K_2SO_4 System

F. Cappeln, N. J. Bjerrum,*,z and I. M. Petrushina*

Materials Science Group, Department of Chemistry, Technical University of Denmark, DK-2800 Lyngby, Denmark

Electrochemical noise measurements have been carried out on AISI347, 10CrMo910, 15Mo3, and X20CrMoV121 steels in molten NaCl-K_2SO_4 at 630°C. Different types of current noise have been identified for pitting, intergranular and peeling corrosion. The corrosion mechanism was the so-called active corrosion (*i.e.*, the corrosion proceeds with no passivation due to the influence of chlorine), characterized by the formation of volatile metal chlorides as a primary corrosion product. It was found possible to obtain an empirical separation of general and intergranular corrosion using kurtosis (a statistical parameter calculated from the electrochemical noise data). It was found that average kurtosis values above 6 indicated intergranular corrosion and average values below 6 indicated general corrosion. The response time for localized corrosion detection in in-plant monitoring was approximately 90 min on this basis. Approximate values of polarization resistances of AISI347 and 15Mo3 steels were determined to be 250 and 100 Ω cm^2, respectively.
 [DOI: 10.1149/1.1928187]

Manuscript submitted March 10, 2004; revised manuscript received January 25, 2005. Available electronically May 26, 2005.

Electrochemical noise measurements (ENMS) is a term used for the registration of small fluctuations in current and potential around a mean value (the steady state), typically at the corrosion potential. The relationship between these current and potential variations is determined by the processes occurring on the electrode. An electrode undergoing localized corrosion displays low-frequency, stochastic transients originating from occurrence of events on the electrode surface. While being random in nature, it still makes intuitive sense to expect a jump in current to be accompanied by a change in potential and visa versa. One application of the ENM technique is to describe this relation between current and potential in terms of a polarization resistance which can be related to the corrosion rate using the procedures developed for potential sweep techniques like steady-state voltammetry.

The first papers concerning electrochemical noise in corrosion were published as early as the 1960s.[1,2] However, breakthrough improvements of the data analysis occurred mostly in the 1990s[3-21] and have established their use and reliability in the present day for many low-temperature applications (construction, nuclear waste barrels, industrial process monitoring, etc.). Some research on high-temperature applications of an ENM technique has been carried out,[22-24] but for now there is no reliable ENM probe for high-temperature corrosion monitoring (waste incineration, fossil fuel combustion, bio-mass combustion, and cofiring combinations thereof).

The present work is a series of laboratory experiments designed to demonstrate whether ENM measurements can be used in the combustion environment when sulfur-containing coal is cofired with chloride-containing biomass (*e.g.*, straw). The eutectic NaCl-K_2SO_4 (40% NaCl by weight) is a model melt for the molten film expected to be formed at superheater tubes at high temperatures. ENM is potentially a very strong tool for monitoring the corrosion, as the technique is well suited for *in situ* real-time measurements. The main goal is to monitor the occurrence of localized corrosion, a major factor in lifetime assessment of process equipment.

Another goal is to measure the corrosion rate. In electrochemical techniques the corrosion resistance of an electrode is commonly expressed as the charge-transfer resistance, or polarization resistance R_p. Bertocci *et al.*[25] investigated how to express this quantity from ENM. They found that for a system of three identical electrodes

$$Lim\left[R_{SN}^{f\to 0}(f)\right] = \sqrt{3}R_p \qquad [1]$$

where f is the frequency and R_{SN} is the spectral noise resistance given by

$$R_{SN} = \sqrt{\frac{\psi_E(f)}{\psi_I(f)}} \qquad [2]$$

where ψ_x is the power spectral density (PSD) of x [x can be either E (potential) or I (current)]. PSDs are calculated from the Fourier-transformed noise data $X(f)$[26]

$$\Psi_x(f) = \frac{2}{T}\frac{1}{N}\sum_{j-1}^{n}|X_j(f)|^2 \qquad [3]$$

where N and T are the number of time records and the time record duration, respectively. The number of individual data points in a time record is n.

Using Eq. 1-3 makes it possible to calculate the polarization resistance from E if the low-frequency limit of $R_{SN}(f)$ can be determined from a R_{SN} *vs.* frequency plot, and that the impedances and noise patterns of the individual electrodes are identical.

Experimental

The laboratory ENM experiments were carried out in a 40:60 NaCl:K_2SO_4 (by weight) melt at 630°C in air atmosphere. The salts (K_2SO_4 Merck pro analysi, min 99%, NaCl Merck pro analysi, min 99.5%) were dried overnight and used with no further purification. The salt was placed in an alumina crucible (stable in this melt) and placed in a cell.[27] The outer casing of the cell was a 50 mm diam quartz tube. The heating was accomplished using a block furnace with temperature regulation within ±1°C.[28] The temperature was continuously monitored using a Chromel-Alumel thermocouple in a protective sheathing. The electrode system consisted of three identical electrodes of the material under investigation.

The electrodes were cut out from superheater tubes, polished, rinsed in ethanol, and dried before use and all had the same physical dimensions. The experiments were carried out on the steel types listed in Table I.

The electrochemical noise data were measured using special equipment and software designed at the Department of Chemistry, Technical University of Denmark. The setup is divided in three units: preamplifier and high-pass filter, main amplifier and low-pass filter, and the computer interface. The electronic filters allow signals above (high-pass) or below (low-pass) a certain frequency to pass but stops other signals. The purpose of the high-pass filter is to eliminate drift in the data. The purpose of the low-pass filter is to remove aliasing effects. The filter had a cutoff value equal to the maximum frequency of the experimental data as given by the sampling rate. The equipment is shown in Fig. 1.

The current preamplifier is an operational amplifier which served as a current-to-voltage converter of 1 V/100 μA or 1 V/1 μA, corresponding to an amplification of 10,000 and 1,000,000, respec-

* Electrochemical Society Active Member.
z E-mail: njb@kemi.dtu.dk

Table I. Steel compositions and electrode area for ENM testing.

Alloy	Composition in wt %	Area (cm^2)
10CrMo910	C 0.06-0.14, Si(max.) 0.5, Mn 0.4-0.8, Al(min.) 4 Cr 2.0-2.5, Mo 0.9-1.1, balance Fe	0.58
15Mo3	C 0.12-0.2, Si(max.) 0.35, Mn 0.4-0.9, Al(min.) 4, Cr < 0.3, Mo 0.25-0.35, Ni < 0.3, balance Fe	0.58
AISI 347	Cr18, Ni10, Nb < 1.2, balance Fe	0.86
X20CrMoV121	C 0.20, Cr 12, Mo 1, B < 1, V 0.25-0.35, Si 0.25-0.35%, balance Fe	1.61

tively. The operator can choose the preferred amplification. The voltage preamplifier is a 30× voltage follower. The noise and drift of both amplifiers are very low and chopper stabilized (Linear Technology type LT1250). The instrumental noise was measured using an ohmic resistor and was found to be orders of magnitude less than the corrosion noise. The high-pass filters for both current and voltage signals are simple resistance-capacitance (RC) elements with time constants of 100 s. Their purpose is to allow high amplification of the noise signal without overloading the amplifiers with dc signal. Drift in the electrochemical system could be a source of such a dc signal.

The low-pass filters are 5th-order, maximally flat, switched-capacitor filters (Linear Technology, type LTC1062). The cutoff frequency can be chosen by the operator as 0.25, 0.5, 1, 2, or 4 Hz. The purpose is to eliminate signals from aliasing. Around the filter circuits are amplifiers with a amplification range from 9× to 300×. The value of the amplification can be set by the operator.

The computer interface consists of an integrating analogue-to-digital (A/D) converter that interfaces with a PC through the serial port.

The data collection program, written in Visual Basic, collects a definite number of current and voltage points (*e.g.*, 1024) with constant intervals (*e.g.*, 0.5 s). This process is repeated with regular intervals. The system consists of three identical steel electrodes. One of these electrodes (electrode 1) is used as a pseudo-reference electrode for potential noise measurement and the current noise is determined by the current between the two other electrodes (electrodes 2 and 3). The noise signal is preamplified, analog filtered to remove aliasing and drifting signals, and finally amplified again. The ENM technique setup is illustrated in Fig. 1.

It is preferable to measure the potential and the current simultaneously (as opposed to sequential measurement) in order to get the best possible data for calculating the electrode impedance, a major

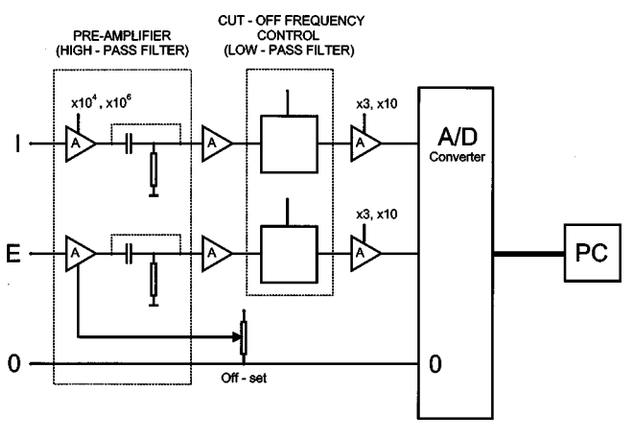

Figure 1. Electronic equipment for EN aquisition and a diagram of the experimental setup used for ENMs.

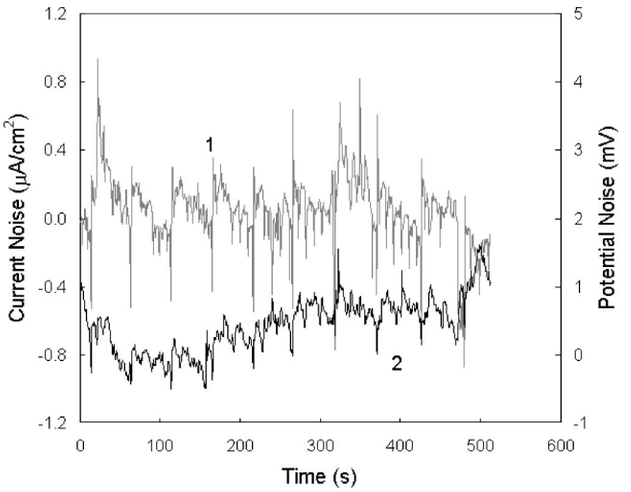

Figure 2. EN from AISI 347 electrodes in 40:60 NaCl-K_2SO_4 at 630°C: (1) current noise and (2) potential noise.

target of the technique. Therefore two identical measuring electrodes are used, identical in the sense that they have the same surface area and were machined with the same procedure and treated the same way before the experiment. During the experiment, differences almost certainly will appear: a stochastic event like pit formation must be expected to happen at a slightly different frequency on one electrode, etc. This factor can be a lifetime limiting factor of an *in situ* ENM probe. However, scanning electron microscopy (SEM) images of the electrodes have shown that no significant differences developed during the experiments.

The third electrode (shown grounded in Fig. 1) is the reference electrode. A true reference electrode like a silver/silver sulfate electrode[27] could also be used. However, in this work it has been chosen to work using a third identical electrode, this being a quasi-reference electrode.

The time records contained 1024 data points of potential and current noise. The sampling frequency was two measurements per second for a total duration of 512 s. For each experiment ten time records were recorded. The transformation to the frequency domain was accomplished by using the fast fourier transform (FFT) algorithm and the PSDs calculated from Eq. 3 (Ref. 6) without the use of additional processing (*i.e.*, no window was applied to the time records before computing the FFT).

The frequency range for the records is $f_{min} = 1/T = 1.95$ mHz and $f_{max} = 1/2\Delta t = 1$ Hz, where T is the time record duration and Δt is the time between sampling of consecutive data points. In order to avoid aliasing the cutoff frequency was set at 1 Hz (thus skipping all contributions from higher frequencies).

Results

The results of the experiments are presented as data mainly obtained under two conditions. The first condition is immediately after the signals have stabilized (the initial formation of corrosion products would usually induce dramatic current and potential changes during the first 30 min after immersion). The second condition is with a stabilized oxide layer typically obtained 24 h after immersion of the electrodes. The recording of ten data sets as required for good precision in the measurements could be accomplished in about 90 min.

AISI 347.— Figure 2 shows the noise patterns observed at an AISI 347 electrode after reaching a stable level. A characteristic pattern of abrupt shifts with approximately 50 s intervals is seen on

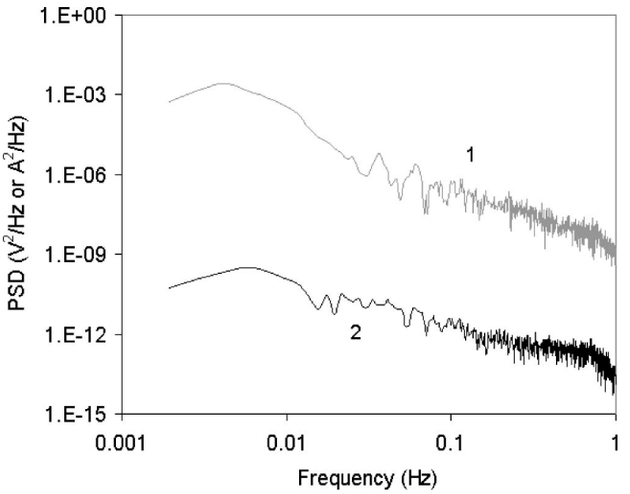

Figure 3. PSDs for current and potential noise from AISI 347 electrodes in 40:60 NaCl-K_2SO_4 at 630°C: (1) current PSD and (2) potential PSD.

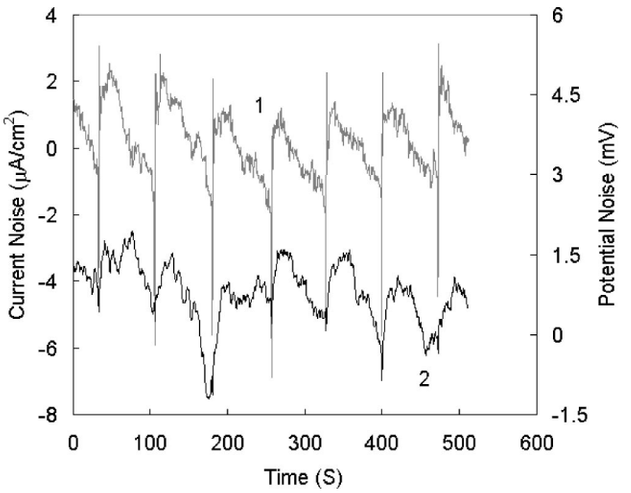

Figure 5. EN from AISI 347 electrodes in 40:60 NaCl-K_2SO_4 at 630°C after 24 h: (1) current noise and (2) potential noise.

a background of fast (the smaller transients) as well as slow events (the gradual change of the baseline). This pattern is seen in the potential as well as the current signal.

The transient is repeated many times, almost periodically, but the interval between bordering events does vary (as you would expect from a stochastic process). These transients are localized corrosion phenomena according to noise theory. In Fig. 3 the PSDs for the current and potential noise are given and the roll-off slopes were determined to be −2. Figure 4 shows a R_{SN} *vs.* frequency plot. It can be seen that the value R_{SN} is largely independent of frequency in the given interval and the assumption that $R_p = R_{SN}$ is thus valid.[21] The value of R_{SN} is approximately 250 Ω cm^2.

After 24 h of immersion the larger magnitude of transients indicate increased localized corrosion (Fig. 5). The frequency domain picture is almost unchanged and R_{SN} is still 250 Ω cm^2 at low frequencies. The constant overall polarization resistance and increased localized corrosion suggest that general corrosion proceeds at a reduced rate due to the formation of an oxide layer.

Figure 6 shows an SEM picture of the corroded AISI 347 electrode. The material has suffered extremely severe intergranular corrosion. Remains of the oxide layer can be seen. Much of this layer was lost as it had extremely poor adherence. The layer mainly consists of iron oxide with traces of chromium oxide. The corrosion product must be expected to have been mostly chlorides which have disappeared due to the volatility of iron and chromium chlorides. The resulting iron oxide could be observed in the melt after the experiments. There was no evidence of a sulfidation process.

The thickness of the AISI 347 samples were 100 μm and the intergranular attack dominated the bulk of the electrodes after 24 h of testing. This loss of structural integrity may have contributed to the poor state of the oxide layer.

10CrMo910.— The electrochemical noise (EN) data obtained for 10CrMo910 are given in Fig. 7. It can be seen that it differs from the EN patterns for AISI 347. The characteristic peaks that are present in AISI 347 EN data are found in the 10CrMo910 current noise data as well, but with a lower frequency of repetition. The SEM image (Fig. 8) indicates a limited intergranular corrosion attack, which is in agreement with this reduced frequency of transients. After 24 h the EN picture is somewhat different: the potential *vs.* time records are now dominated even more by a single transient, while the "intergranular" transients have disappeared from the current noise (Fig. 9). It is likely that the significant potential changes are caused be

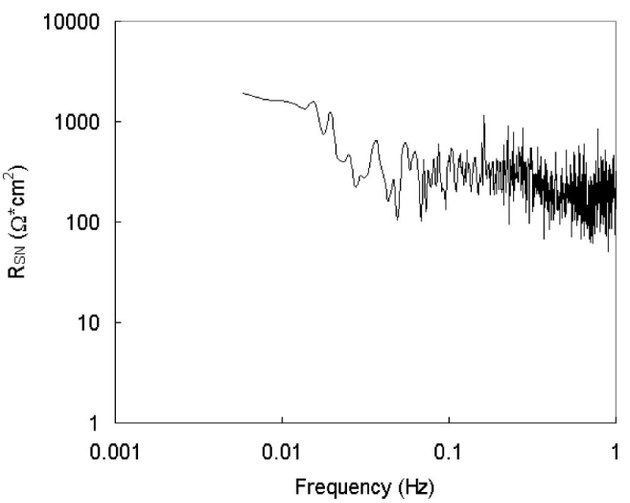

Figure 4. R_{SN} *vs.* frequency from AISI 347 electrodes in 40:60 NaCl-K_2SO_4 at 630°C.

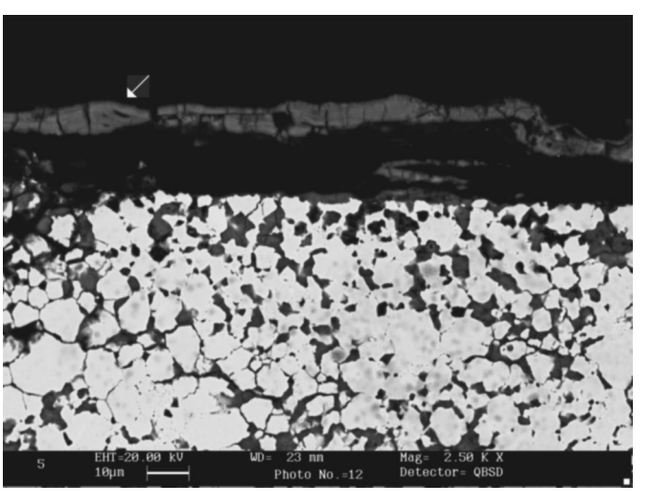

Figure 6. SEM picture of a corroded AISI 347 electrode. The arrow indicates the remains of the oxide layer.

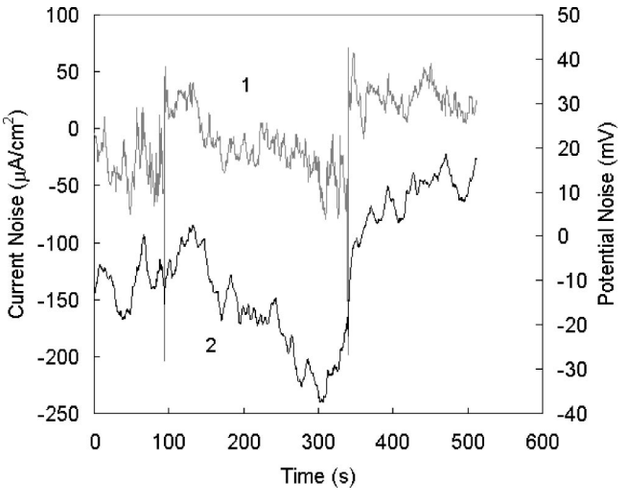

Figure 7. EN from 10CrMo910 electrodes in 40:60 NaCl-K_2SO_4 at 630°C: (1) current noise and (2) potential noise.

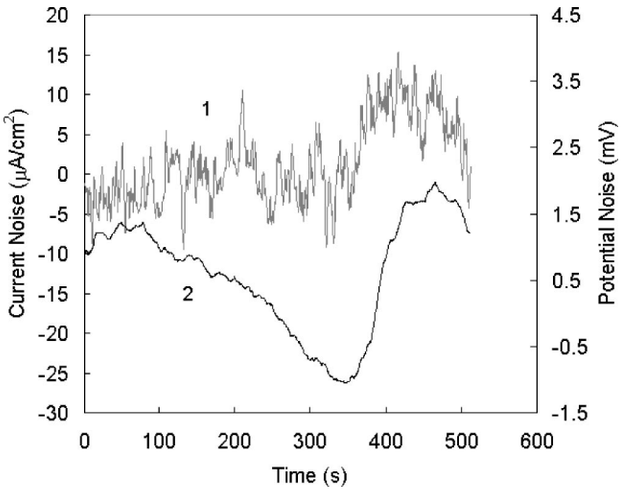

Figure 9. EN from 10CrMo910 electrodes in 40:60 NaCl-K_2SO_4 at 630°C after 24 h: (1) current noise and (2) potential noise.

peeling of the oxide layer from the steel surface. The peeling can be provoked by formation of volatile chlorides during corrosion.[29]

15Mo3.— The typical noise on 15Mo3 low-alloy steel is shown in Fig. 10. The pattern is similar to what can be expected from pitting corrosion,[30] but SEM analysis did not reveal any signs of it. In fact, there is no indication of localized corrosion at all. However, a broken and nonadherent oxide layer is observed after corrosion (Fig. 11). The results are similar to what was observed on 10CrMo910 in the sense that a few large transients dominate the picture for the potential noise. As earlier, it is supposed that these few major transients are the result of parts of the oxide layer falling off the electrodes because of volatile chloride formation. This formation of volatile chloride can clearly be seen in Fig. 11. The outer oxide layer is a mixture of iron oxide and sulfide (the light areas in Fig. 11 are the sulfide, as seen from the element mapping in Fig. 12). From the SEM element mapping (Fig. 12) another important observation can be made: Near the electrode surface a mixture of iron oxide and iron chloride is found. Normally, such iron chloride would vaporize but in this SEM picture we see a proof of its formation.

The formation of iron (and chromium) chlorides is the result of inward diffusion of chloride ions (and water and oxygen if present as in this case) through the porous oxide layer and an electrochemical reaction[31]

$$\text{Cathodic:} O_2 + 2H_2O + 4e^- \rightarrow 4OH^- \quad [4]$$

$$\text{Anodic:} Fe + 3Cl^- \rightarrow FeCl_3 + 3e^- \quad [5]$$

$$\text{Total:} 3O_2 + 6H_2O + 4Fe + 12Cl^- \rightarrow 4FeCl_3 + 12OH^- \quad [6]$$

The final corrosion product is Fe_2O_3

$$4FeCl_3 + 3O_2 \rightarrow 2Fe_2O_3 + 6Cl_2 \quad [7]$$

The formation of volatile chloride (boiling point for $FeCl_3$ is 315°C[32]) results in a breakdown of the oxide layer as it escapes as a bobble. This removes the diffusional barrier for H_2O/O_2 and Cl^- and enhances the corrosion rate dramatically until a new oxide layer can be formed. This is the pattern reflected in the EN data. The mechanism of forming chlorine gas available for further corrosion is well known and the term "active corrosion" has been proposed by Grabke.[33,34]

The PSD roll-off slopes calculated from the data in Fig. 11 are −2. R_{SN} was determined to 110 Ω cm^2 with the conditions of $R_{SN} = R_p$ fulfilled. The data after 24 h of immersion (Fig. 13) shows that in this case the EN is basically unchanged from the

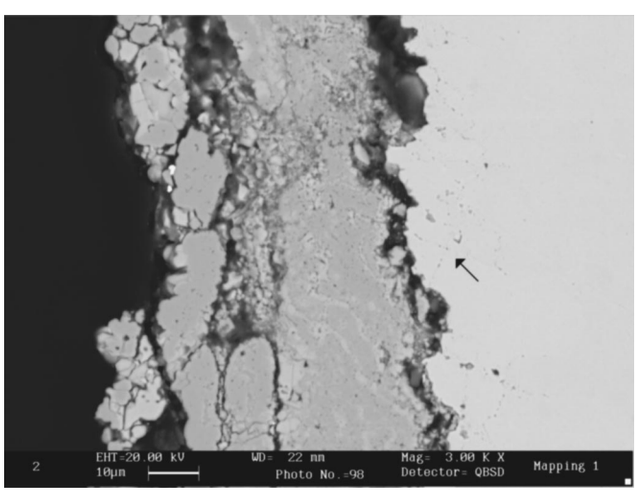

Figure 8. SEM picture of a corroded 10CrMo910 electrode. The arrow indicates the location of the limited intergranular attack.

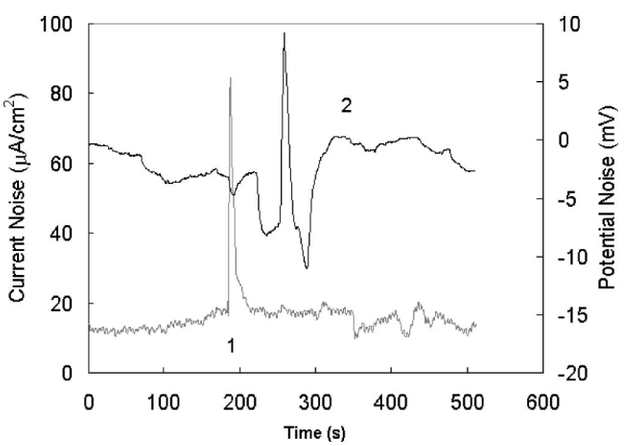

Figure 10. EN from 15Mo3 electrodes in 40:60 NaCl-K_2SO_4 at 630°C: (1) current noise and (2) potential noise.

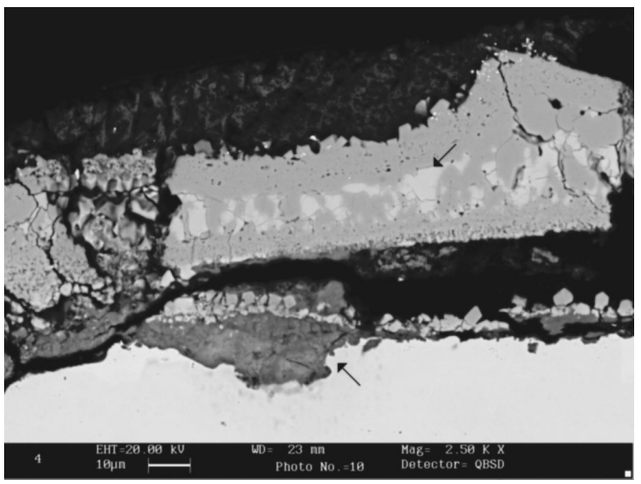

Figure 11. SEM picture of a corroded 15Mo3 electrode. The top arrow indicates the light areas in the oxide layer which have been identified as iron sulfide. The bottom arrow indicates the area identified as iron chloride. Identifications were made using X-ray element analysis (EDAX).

situation immediately after stable levels are obtained (Fig. 11). In the frequency domain the R_{SN} does not reach a limiting value at low frequencies, but the value is above 100 Ω cm^2. The roll-off slopes have an unusual value of −3. It can be seen that the peeling process causes a state of nonequilibrium. As the oxide layer on one of the three electrodes breaks, the result is a large transient which lasts for as long as it takes the oxide layer to reform.

X20CrMoV121.— The noise records for the X20CrMoV121 steel are somewhat different from the other types of steel investigated (Fig. 14). The major current transients observed on the first recordings are abrupt changes in the current and what appears to be an exponential return to the equilibrium values. Such behavior is commonly found in connection with pitting corrosion.[30] An SEM image, shown in Fig. 15, confirms that this is the case, as shallow pits are formed on the electrode surface. An important aspect of this pitting formation is that it is likely to develop differences in electrode properties over time. Most notably the electrode impedance will be different from a pitted electrode and a nonpitted electrode, which in turn may lead to preferential pitting of the already attacked electrode. This behavior results in a completely different appearance of the voltage and current noise as seen in Fig. 14. The current noise shows positive and negative transients consistent with pitting on

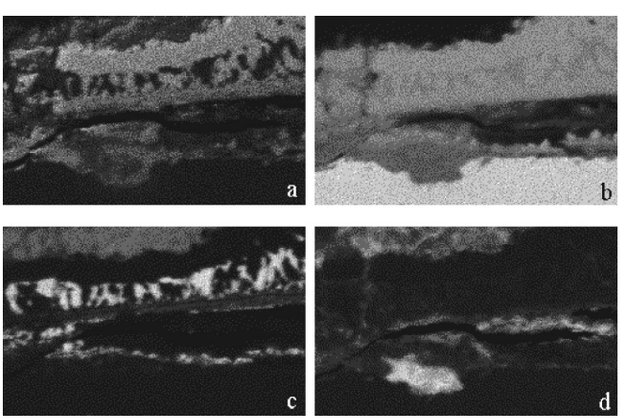

Figure 12. SEM element mapping of oxygen, iron, sulfur, and chlorine corresponding to Fig. 11: (a) oxygen, (b) iron, (c) sulfur, and (d) chlorine.

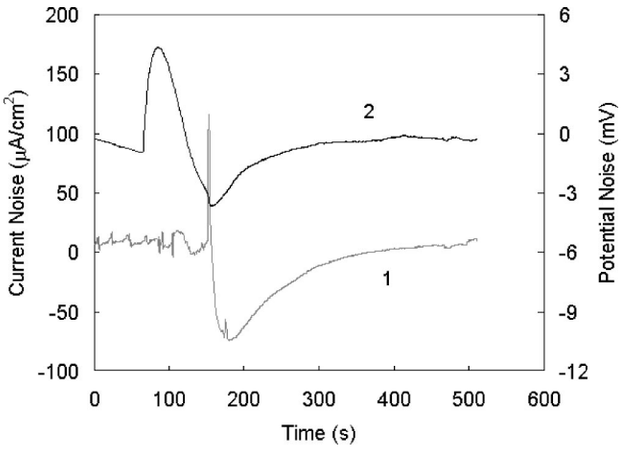

Figure 13. EN from 15Mo3 electrodes in 40:60 NaCl-K_2SO_4 at 630°C after 24 h: (1) current noise and (2) potential noise.

both the current measuring and pseudo-reference electrodes. However, the potential noise shows no sign of pitting corrosion in progress. This is most likely due to a passivation of the potential measuring electrode. From the frequency domain data shown in Fig. 16 and 17, it can be seen that the spectral noise resistance actually drops as the frequency is decreased. Equation 1 requires the electrodes to be identical. It does not apply to this system and any simple relationship between R_{SN} and R_p cannot be expected. The effect is also seen in the frequency domain where the PSD(E) roll-off slope is close to zero, while the current roll-off slope is −2. The SEM image (Fig. 15) shows the pseudo-reference electrode. After 24 h the pattern is the same, although less obvious (Fig. 18).

Discussion

A brief summary of the results is given in Table II. In this table, the "$R_{SN} = R_p$?" column indicates whether the theoretical assumptions for setting $R_p = R_{SN}$ are fulfilled or not. There are two cases that do not follow this assumption. First, if the corrosion is diffusion limited the R_{SN} *vs.* frequency plot will show a negative slope no matter how low frequencies are investigated. This is known from impedance spectroscopy where the corresponding feature is termed the Warburg impedance, a diffusion factor that dominates the impedance at lower frequencies and results in a slope of −1.[35] Second, if

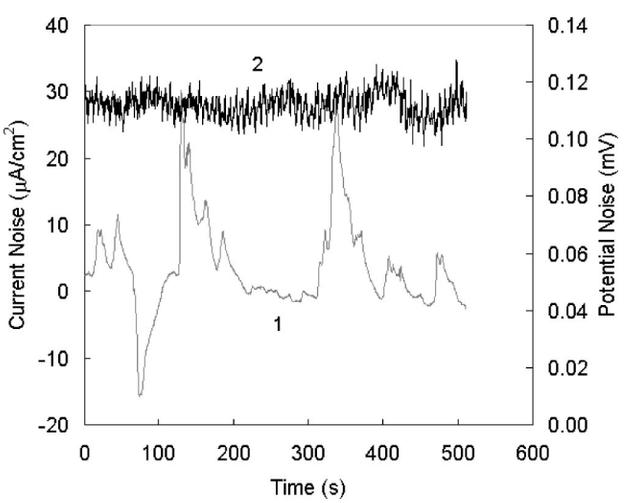

Figure 14. EN from X20CrMoV121 electrodes in 40:60 NaCl-K_2SO_4 at 630°C: (1) current noise and (2) potential noise.

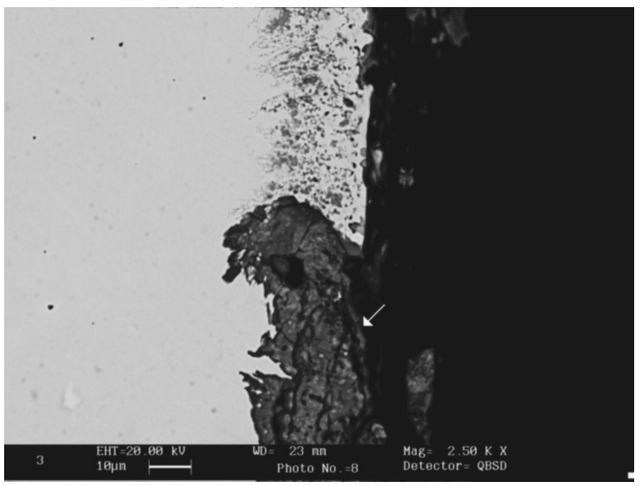

Figure 15. SEM picture of a corroded X20CrMoV121 electrode. The arrow indicates a shallow pit.

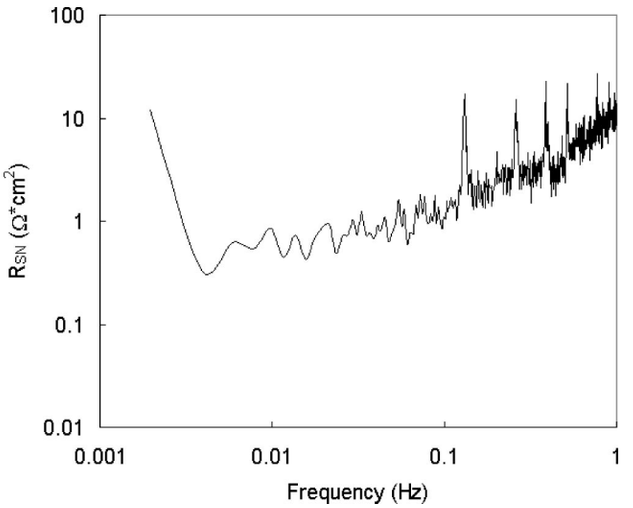

Figure 17. R_{SN} *vs.* frequency from X29 electrodes in 40:60 NaCl-K_2SO_4 at 630°C.

the electrodes develop significant changes between each other during the course of corrosion, the condition of identically noisy electrodes will not be fulfilled as required. Futhermore, it is known that in the case of pitting corrosion the impedance spectrum (*i.e.*, the R_{SN} *vs.* frequency plot) can be of a type which results in the absence of dependance between R_{SN} and R_p.[36] Except for these cases the values of the polarization resistance could be evaluated.

The amount of data generated during monitoring is large. This situation is common for implementation of the ENM technique. Various steps have to be taken in order to simplify the output so that a corrosion expert would not be required to extract the information of each time record. Neural network software systems seem promising as they are well suited for pattern recognition tasks.[37,38]

However, this work confines itself to the discussion of suitable statistic parameters for such a network (statistical parameters will have to form the backbone of an automated pattern recognition scheme). The usefulness of the so-called pitting index (PI) which has been applied to other cases[22] was found to make an insufficient and unreliable distinction between the different morphologies. Likewise, analysis of the variance and skewness of the dataset proved insufficient for the present data. More successful was the application of the so-called kurtosis (g_2). Its use has been previously suggested in literature[37-39] and it is a parameter that indicates the "peakedness" of a data set. A kurtosis statistic close to zero indicates a data set close to a normal distribution, while positive values indicate a data set with many transients.[40] It is given by the following equation

$$g_2 = \frac{m_4}{(m_2)^2} = \frac{\frac{1}{n}\sum_{t=1}^{n}(x_t - x_{av})^4}{\left(\frac{1}{n}\sum_{t=1}^{n}(x_t - x_{av})^2\right)^2} \quad [8]$$

where $(x_t - x_{av})$ is the difference between the individual data points (x_t) and the average of the set (x_{av}). In other words, g_2 is equal to the fourth moment (m_4) divided by the variance (m_2) squared. It has no unit. This parameter has been calculated for the data provided in order to find an objective criterion for evaluating from the noise data if intergranular corrosion was in progress or not. The lack of stationary corrosion conditions in all cases (*i.e.*, not for 10CrMo910 and

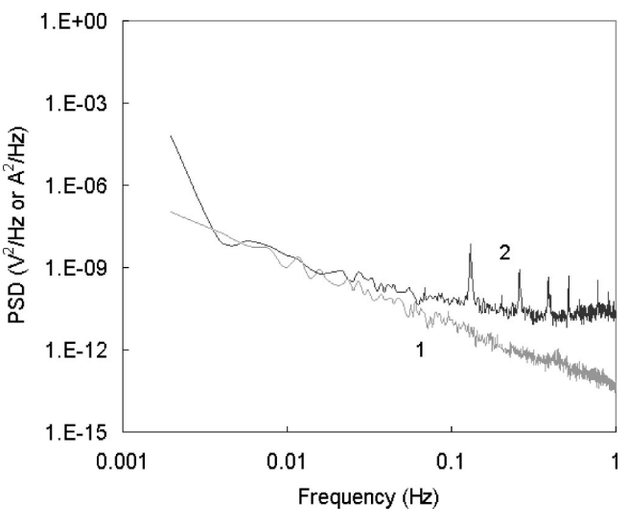

Figure 16. PSDs for current and potential noise from X20CrMoV121 electrodes in 40:60 NaCl-K_2SO_4 at 630°C: (1) current PSD and (2) potential PSD.

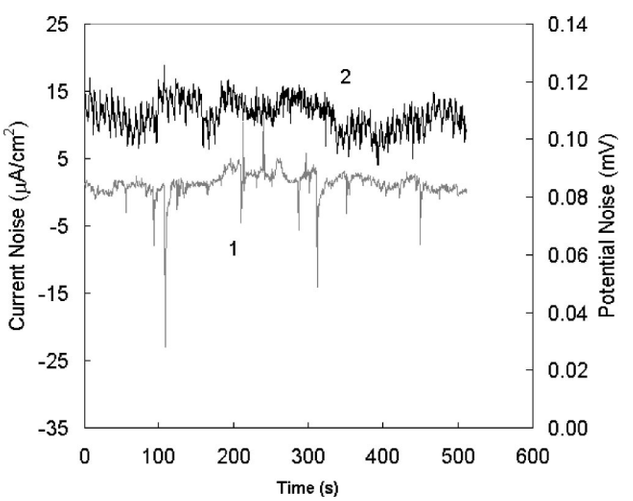

Figure 18. EN from X20CrMoV121 electrodes in 40:60 NaCl-K_2SO_4 at 630°C after 24 h: (1) current noise and (2) potential noise.

Table II. Summary of laboratory ENM experiments.

Steel	Time	Roll-off slope PSD (E)	Roll-off slope PSD (I)	Potential noise transients	Current noise transients	R_{SN}	Morphology as determined by SEM	$R_{SN} = R_P$?
AISI 347	Day 0	−2	−2	Abrupt (50)[a]	Abrupt (50)[a]	250	Severe intergranular, loose scale	Yes
AISI 347	Day 1	−2	−1.5	Abrupt (70)[a]	Abrupt (70)[a]	250	Severe intergranular, loose scale	Yes
10CrMo910	Day 0	−2	−1	Many[b]	Abrupt (200)[a]	Unknown	Limited intergranular	No
10CrMo910	Day 1	−2	−2	Few[c]	No pattern[d]	Unknown	Limited intergranular	No
15Mo3	Day 0	−2	−2	Few[c]	Few[c]	110	Uniform corrosion	Yes
15Mo3	Day 1	−3	−3	Few[c]	Few[c]	100	Uniform corrosion	Yes
X20CrMoV121	Day 0	0	−2	No pattern[d]	Few[c]	Unknown	Shallow pitting	No
X20CrMoV121	Day 1	−1	−2	No pattern[d]	Many[b]	Unknown	Shallow pitting	No

[a] Abrupt transients. The approximate period is indicated in parantheses.
[b] Many transients with a few major transients dominating.
[c] Few transients with a few major transients dominating.
[d] Many transients without any apparent pattern.

Table III. Kurtosis for different steels.

Test	AISI 347	X20CrMoV121	15Mo3
1	11.94	8.93	6.87
2	11.12	7.91	5.81
3	11.25	7.74	5.33
4	8.43	6.97	4.93
5	7.74	5.56	3.48
6	6.54	4.79	4.26
7	6.21	3.80	3.90
8	6.14	3.20	3.07
9	5.33	2.48	2.50
10	4.77	1.77	2.27
Average	7.95	5.32	4.24

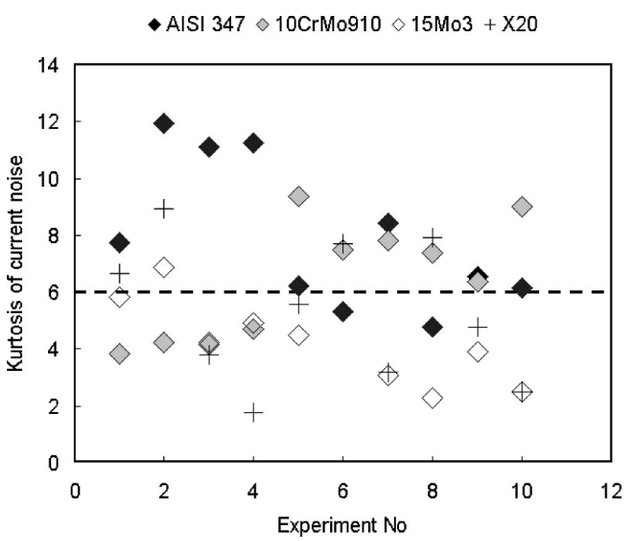

Figure 19. Kurtosis values calculated from the current noise signal (as seen in Table III). The cutoff value is indicated: kurtosis values above 6.0 indicate intergranular corrosion.

X20CrMoV121) resulted in the current noise data being far more reliable for statical interpretations than the potential noise data. It was therefore chosen to present kurtusis evaluations for current data only for clarity.

Table III and Fig. 19 show the kurtosis values for current noise after 24 h of immersion. In Table III the values have been arranged by the size of the kurtosis, largest to smallest, while Fig. 19 shows the data as they were obtained chronologically.

This parameter shows considerable potential as the trends are that the intergranular corrosion gives higher values of kurtosis. The (empirical) cut value is around $g_2 = 6$. Average values of g_2 less than 6 indicate general corrosion, and average values of g_2 higher 6 indicate intergranular corrosion. However, the deviations from this average value, indicated in Fig. 19, suggest that this separation of corrosion types requires about ten time records for a reliable determination of the average g_2 level. This means that the indication time is between 1 and 2 h. If a faster indication is required other statistical quantities will need to be considered. The reason the g_2 values for 10CrMo910 and 15Mo3 are partly above the cut value is that a limited localized corrosion occurs even when intergranular corrosion does not occur, as discussed earlier. The kurtosis value for the pitting corrosion of X20CrMoV121 was inconclusive.

Conclusions

Corrosion of steels has been studied in the K_2SO_4-NaCl eutectic melt at 630°C using the EN technique. The molten K_2SO_4-NaCl mixture is a simulation of the molten salt film formed on superheater tubes during cofiring of straw and coal.

EN data have been collected for four different types of steel which can be used as superheater construction materials. It has been shown that the EN technique can predict the corrosion rate if the low-end frequency limit of the impedance can be reached and the three identical electrodes used in the experiments are, in fact, corroding in the same way (identical impedances). An example of this can be seen in Fig. 4. Moreover, the ENM data makes it possible to distinguish between different corrosion morphologies. In the present work it has been demonstrated that a characteristic transient (shown in, for example, Fig. 2 and 5) can be ascribed to intergranular corrosion, which is the main localized corrosion type found in chloride-containing systems at high temperatures.[41] SEM and ENM measurements indicate shallow pitting of X20CrMoV121 electrodes. The requirement of at least ten individual recordings in order to determine a realiable average value for the kurtosis parameter results in a response time of around 90 min.

Acknowledgment

This investigation has been supported by a Danish project between The Technical University of Denmark, Energi E2 and ELSAM (BRO-19328), and a European project (ECSC contract no. 7220-PR-080).

The Technical University of Denmark assisted in meeting the publication costs of this article.

References

1. T. Hagyard and J. R. Williams, *Trans. Faraday Soc.*, **157**, 2288 (1961).
2. W. P. Iverson, *J. Electrochem. Soc.* **115**, 617 (1968).
3. J. Hickling, J. Goellner, A. Burkert, and A. Heyn, *Corrosion '98*, NACE, Paper no. 385 (1998).
4. J. L. Dawson, *Electrochemical Noise Measurement for Corrosion Applications, ASTM STP 1277*, J. R. Kearns, J. R. Scully, P. R. Roberge, D. L. Reichert, and J. L. Dawnson, Editors, pp. 3-35, American Society for Testing and Materials, West Conshohocken, PA (1996).
5. F. Huet, U. Bertocci, C. Gabrielli, and M. Keddam, in *Proceedings of Corrosion '97*, NACE, pp. 11-30 (1997).
6. C. Gabrielli, F. Huet, and M. Keddam, *NATO ASI Ser., Ser. E* **203**, 135 (1991).
7. A. Legat and V. Dolecek, *J. Electrochem. Soc.* **142**, 1851 (1995).
8. U. Bertocci and F. Huet, *Corrosion (Houston)* **51**, 131 (1995).
9. F. Almeraya-Calderon, A. Martinez-Villafañe, and J. G. Gonzalez-Rodriguez, *Br. Corros. J., London* **33**, 288 (1998).
10. M. L. Benish, J. Sikora, B. Shaw, E. Sikora, M. Yaffe, A. Krebs, and G. Martinchek, *Corrosion '98*, NACE, Paper no. 370 (1998).
11. Y. C. Lu and M. B. Ives, in *Critical Factors in Localized Corrosion*, P. M. Natishan, Editor, PV 96-95, p. 253,The Electrochemical Society Proceedings Series, Pennington, NJ (1996).
12. F. Mansfeld and H. Xiao, *Electrochemical Noise Measurement for Corrosion Applications*, ASTM STP 1277, J. R. Kearns, J. R. Scully, P. R. Roberge, D. L. Reichert, and J. L. Dawnson, Editors, pp. 59-78, American Society for Testing and Materials, West Conshohocken, PA (1996).
13. R. Ke and R. Alkire, *J. Electrochem. Soc.* **142**, 4056 (1995).
14. Z. Wang, X. Wei, J. Li, and W. Ke, *J. Mater. Sci. Technol.* **12**, 291 (1996).
15. L. Mészáros, G. Mészáros, A. Pirnát, and B. Lengyel, *J. Electrochem. Soc.* **143**, 3597 (1996).
16. Y. F. Cheng, J. L. Luo, and M. Wilmott, *Corrosion '98*, NACE, Paper no. 389 (1998).
17. F. Mansfeld and H. Xiao, *J. Electrochem. Soc.* **140**, 2205 (1993).
18. D. A. Eden, *J. Electrochem. Soc.* **141**, 1402 (1994).
19. Y. Watanabe and T. Kondo, *Corrosion '98*, NACE, Paper No. 376 (1998).
20. D. A. Reichert, *Electrochemical Noise Measurement for Corrosion Applications*, ASTM STP 1277, J. R. Kearns, J. R. Scully, P. R. Roberge, D. L. Reichert, and J. L. Dawnson, Editors, pp. 79-89, American Society for Testing and Materials, West Conshohocken, PA (1996).
21. U. Bertocci, C. Gabrielli, F. Huet, M. Keddam, and P. Rousseau, *J. Electrochem. Soc.* **144**, 37 (1997).
22. D. A. Eden, D. G. John, and J. L. Dawson, Int. Pat. WO 87/07022 (1987).
23. Electric Power Research Institute (EPRI) Report, EPRI TR-101799, Project 1403-48 (1992).
24. D. M. Farell, W. M. Cox, F. H. Stott, D. A. Eden, J. L. Dawson, and G. C. Wood, *High Temperature Technol.*, **3**, 15 (1985).
25. U. Bertocci, C. Gabrielli, F. Huet, and M. Keddam, *J. Electrochem. Soc.* **144**, 31 (1997).
26. J. S. Bendat and A. G. Piersol, *Engineering Applications of Correlation and Spectral Analysis*, John Wiley & Sons, Inc., New York (1980).
27. I. M. Petrushina, N. J. Bjerrum, R. W. Berg, and F. Cappeln, *J. Electrochem. Soc.* **144**, 532, (1997).
28. H. A. Andreasen, N. J. Bjerrum, and C. E. Foverskov, *Rev. Sci. Instrum.* **48**, 1340 (1977).
29. F. Cappeln, I. Petrushina, and D. Baxter, *Progress in Molten Salt Chemistry*, **1**, 127 (2000).
30. A. Bautista, U. Bertocci, and F. Huet, *J. Electrochem. Soc.* **148**, B412 (2001).
31. A. Nishikata, Y. Shimatani, and S. Haruyama, *Nippon Kinzoku Gakkaishi* **48**, 705 (1984).
32. *CRC Handbook of Chemistry and Physics*, 63rd ed., Boca Raton, FL (1982).
33. H. J. Grabke, *Incinerating Municipal Industrial Waste: Fireside Problems and Prospects for Improvement*, p. 161, Hemisphere, New York (1991).
34. H. J. Grabke, E. Reese, and M. Spiegel, *Molten Salt Forum, Molten Salt and Technology 5*, p. 405, Trans Tech Publications, Zurich, Switzerland (1998).
35. R. Greef, R Peat, L. M. Peter, D. Pletcher, and J. Robinson, *Instrumental Methods in Electrochemistry*, Ellis Horwood, Limited, England (1990).
36. W. A. Badaway, S. S. El-Egamy, and A. S. El-Azab, *Corros. Sci.* **37**, 1969 (1995).
37. S. Reid, G. E. C. Bell, and G. L. Edgemon, *Corrosion 98*, NACE, Paper no. 176 (1998).
38. S. A. Reid and D. A. Eden, U.S. Pat. 6,264,824 (2001).
39. D. A. Eden, *Corrosion '98, NACE*, Paper no. 386 (1998).
40. J. D. Brown, *JALT Testing and Evaluation SIG Newsletter*, **1**, 16 (1997); Internet location: http://www.jalt.org/test/bro_1.htm
41. G. Y. Lai, *High-Temperature Corrosion of Engineering Alloys*, ASM International, Materials Park, OH (1990).